

Estimating 3D orientation of a body segment during running using one inertial sensor and assuming a cyclical nature of the movement

Romano Ferla¹

Abstract—Long distance running involves high risks of injuries for which it is important to identify and detect such risks during running. A sensing system consisting out of inertial sensors is chosen, though these are sensitive to errors. The estimated 3D orientation should be acquired drift free. By exploiting the cyclical behaviour of running, three drift reduction methods are proposed to estimate the 3D orientation. The first method will remove the mean of the angular velocity. The second method rotates the angular velocity first to the axis on the knee perpendicular to the sagittal plane. The third method will set a custom offset on the angular velocity such that the drift is minimized. The results show that exploiting the cyclical behaviour of walking and running can help to reduce the drift when the 3D orientation is estimated. It is shown that the same phases in different gait cycles have a similar estimate of the 3D orientation. A custom offset, for both method 2 as for method 3, delivers the best results. An accuracy of at least 2 degrees can be achieved for both walking and running. It is expected that with this method, sensors can operate individually on any position on the body during running without the need of extensive calibration beforehand.

I. INTRODUCTION

Long distance running involves high risks of injuries [1]. It is important that such risks are identified and detected to inform the individual runner during running. These risks might be caused by a less optimal running technique due to fatigue. To detect the change in technique and the additional risks, the movements of the subject should be analyzed, which is done with human motion tracking. There are a number of tracking solutions, each with their advantages and disadvantages. The sensors must be self-contained due to the ambulant behaviour of running and may not be a burden to the runner themselves. Therefore a light weight and small sized system is required.

Due to the constraints mentioned, a minimal set of three inertial sensors for this system is chosen. Two sensors will be placed on each tibia and one for on the sacrum. The tibia is a bone positioned in the front of the lower leg and provides a rigid fixation point for inertial sensors as there is only a minimum amount of soft tissue between the bone and the skin. As this bone is adjacent to the knee it is expected to get information about the knee too, which is valuable information as a significant amount of injuries involves the knee [2]. The sacrum is chosen as it is near the center of mass while standing and therefore interesting to know what happens during long distance running [3]. Note that the research focuses on the usage of one inertial sensor.

¹R. Ferla is a bachelor student with Faculty of Electrical Engineering, Mathematics and Computer Science, University of Twente, 7500 AE Enschede, The Netherlands

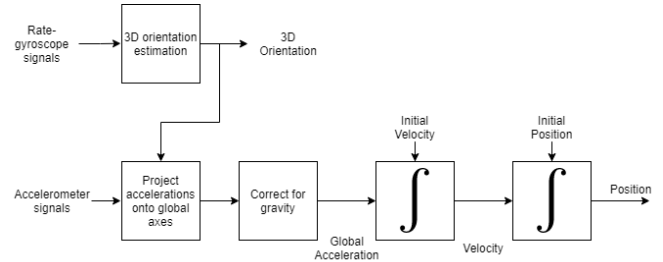


Fig. 1. The Strapdown Inertial Navigation Algorithm. Source: Adapted from [5]

Inertial sensors (often referred to as Inertial Measurement Units, (IMU)'s) are microelectromechanical systems (MEMS) sensors and often lightweight and small in size. In addition to that the sensors are self-contained, they can be used individually to calculate the 3D orientation, acceleration, velocity and position without the use of any external system. An inertial sensor consists of a combination of accelerometers, gyroscopes and are sometimes combined with magnetometers. Often these sensors are able to measure in three dimensions [4]. To acquire the among others the orientation and position, a strapdown inertial navigation algorithm can be used. The algorithm utilizes the gyroscope signals to acquire an estimated 3D orientation to rotate the accelerometer signals to the global coordinate system. After this the gravity can be subtracted and velocity and position can be derived. This is shown in Fig. 1.

However, it is known that using numerical integration is inherently prone to errors, often labeled as integration drift. Gyroscopes and accelerometers are subject to offsets, thermo-mechanical white noise, flicker noise, temperature effects and calibration errors. When integrated, most errors become significant over a certain amount of time as their errors are add up. The offsets, also known as bias, and the thermo-mechanical white noise limit the performance the most [5].

Even in modern systems the integration drift is still a problem and should be corrected for. The correction can either be applied based on sensor fusion or with domain specific assumptions. Sensor fusion uses an additional sensing system with a Kalman filter or a variation on it to combine it with the data of the inertial sensors. A downside of this method is that extra sensors are needed, counteracting the minimal sensor set and therefore the burden to the runner [6].

A domain specific assumption which is often used during walking is the zero velocity update, which assumes that the velocity of (a sensor on) the foot is zero during the stance

Estimating 3D orientation of a body segment during running using one inertial sensor and assuming a cyclical nature of the movement

Romano Ferla¹

Abstract—Long distance running involves high risks of injuries for which it is important to identify and detect such risks during running. A sensing system consisting out of inertial sensors is chosen, though these are sensitive to errors. The estimated 3D orientation should be acquired drift free. By exploiting the cyclical behaviour of running, three drift reduction methods are proposed to estimate the 3D orientation. The first method will remove the mean of the angular velocity. The second method rotates the angular velocity first to the axis on the knee perpendicular to the sagittal plane. The third method will set a custom offset on the angular velocity such that the drift is minimized. The results show that exploiting the cyclical behaviour of walking and running can help to reduce the drift when the 3D orientation is estimated. It is shown that the same phases in different gait cycles have a similar estimate of the 3D orientation. A custom offset, for both method 2 as for method 3, delivers the best results. An accuracy of at least 2 degrees can be achieved for both walking and running. It is expected that with this method, sensors can operate individually on any position on the body during running without the need of extensive calibration beforehand.

I. INTRODUCTION

Long distance running involves high risks of injuries [1]. It is important that such risks are identified and detected to inform the individual runner during running. These risks might be caused by a less optimal running technique due to fatigue. To detect the change in technique and the additional risks, the movements of the subject should be analyzed, which is done with human motion tracking. There are a number of tracking solutions, each with their advantages and disadvantages. The sensors must be self-contained due to the ambulant behaviour of running and may not be a burden to the runner themselves. Therefore a light weight and small sized system is required.

Due to the constraints mentioned, a minimal set of three inertial sensors for this system is chosen. Two sensors will be placed on each tibia and one for on the sacrum. The tibia is a bone positioned in the front of the lower leg and provides a rigid fixation point for inertial sensors as there is only a minimum amount of soft tissue between the bone and the skin. As this bone is adjacent to the knee it is expected to get information about the knee too, which is valuable information as a significant amount of injuries involves the knee [2]. The sacrum is chosen as it is near the center of mass while standing and therefore interesting to know what happens during long distance running [3]. Note that the research focuses on the usage of one inertial sensor.

¹R. Ferla is a bachelor student with Faculty of Electrical Engineering, Mathematics and Computer Science, University of Twente, 7500 AE Enschede, The Netherlands

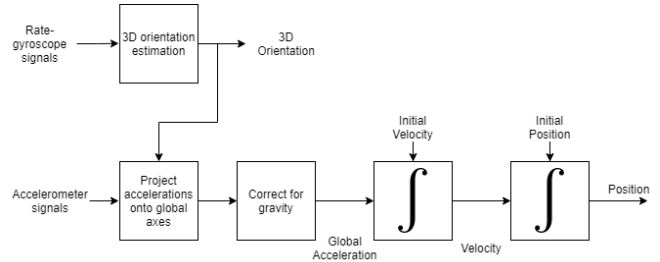


Fig. 1. The Strapdown Inertial Navigation Algorithm. Source: Adapted from [5]

Inertial sensors (often referred to as Inertial Measurement Units, (IMU)'s) are microelectromechanical systems (MEMS) sensors and often lightweight and small in size. In addition to that the sensors are self-contained, they can be used individually to calculate the 3D orientation, acceleration, velocity and position without the use of any external system. An inertial sensor consists of a combination of accelerometers, gyroscopes and are sometimes combined with magnetometers. Often these sensors are able to measure in three dimensions [4]. To acquire the among others the orientation and position, a strapdown inertial navigation algorithm can be used. The algorithm utilizes the gyroscope signals to acquire an estimated 3D orientation to rotate the accelerometer signals to the global coordinate system. After this the gravity can be subtracted and velocity and position can be derived. This is shown in Fig. 1.

However, it is known that using numerical integration is inherently prone to errors, often labeled as integration drift. Gyroscopes and accelerometers are subject to offsets, thermo-mechanical white noise, flicker noise, temperature effects and calibration errors. When integrated, most errors become significant over a certain amount of time as their errors are add up. The offsets, also known as bias, and the thermo-mechanical white noise limit the performance the most [5].

Even in modern systems the integration drift is still a problem and should be corrected for. The correction can either be applied based on sensor fusion or with domain specific assumptions. Sensor fusion uses an additional sensing system with a Kalman filter or a variation on it to combine it with the data of the inertial sensors. A downside of this method is that extra sensors are needed, counteracting the minimal sensor set and therefore the burden to the runner [6].

A domain specific assumption which is often used during walking is the zero velocity update, which assumes that the velocity of (a sensor on) the foot is zero during the stance

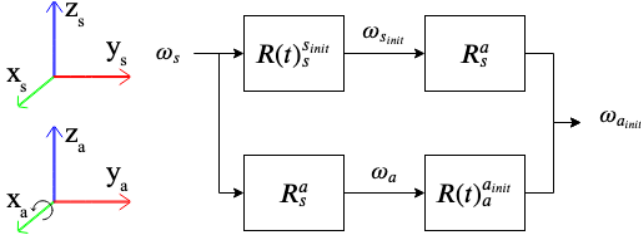


Fig. 2. The sensor body frame Ψ^s with angular velocity ω_s is aligned with the sensor body. The 3D orientation can be estimated with the use of eq. (1). By using this time dependent rotation matrix, the angular velocity ω_{sinit} with respect to the initial orientation can be calculated. ω_s may be rotated first to the partial segment frame Ψ^a , such that the axis x_a resembles with the axis on the knee perpendicular to the sagittal plane. In a drift-free estimated 3D orientation ω_{ainit} is identical for both approaches

phase. This method is less suitable for running at higher velocities, as the stance phase is too short [7], [8], [9]. In some work periodic movements are exploited for analytical integration using adaptive filtering methods, such as the weighted-frequency Fourier linear combiner (WFLC) or the band-limited multiple Fourier linear combiner (BMFLC). The measured signals can be modelled with these filters and analytically integrated with the Fourier series. Both are not verified for running [6], [10].

To the best of the author's knowledge, there currently does not seem to be a solution for the drift-free 3D orientation estimation for periodic movements with a single IMU. Therefore a new method in drift cancellation is required. In this research three new methods of drift cancellation are proposed by exploiting the cyclical nature of running. The main idea revolves around the following assumption: If a person is running with a constant speed along a straight line, the gait cycles and its values should be similar to respectively the other gait cycles and its values. With such a method sensors can operate individually on any position on the body during running without the need of extensive calibration beforehand. This work focuses on the drift-free estimation of 3D orientations.

This leads to the research question: How can the cyclical nature of running be used to acquire drift-free estimates of the 3D orientation using a single inertial sensor?

II. METHOD

This section will provide the necessary theory and present the methods to cancel the drift with the use of the cyclic behavior. First, the theory about the estimation of the 3D orientation is given in Section II-A. Analysis of the influence of bias on the drift is shown in II-B. The three methods for drift compensation using cyclical behaviour are proposed in Section II-C. Information about the experimental measurement is elaborated on in Section II-D and finally the analysis of the results is explained in Section II-E.

A. Orientation and integration

The orientation estimation of the sensor body frame Ψ^s depends on previous rotations, as the rotation from the sensor body frame Ψ^s to the sensor body frame with respect to the initial orientation Ψ^{sinit} is time dependent. Therefore the

rotation is done with an adaptation to the differential equation expressed in eq. (1) [11].

The time dependent rotation matrix \mathbf{R}_s^{sinit} expresses the rotation from the sensor body frame Ψ^s to the sensor body frame with respect to the initial orientation Ψ^{sinit} . $\dot{\mathbf{R}}_s^{sinit}$ is the time derivative of \mathbf{R}_s^{sinit} . $\tilde{\omega}_s^{s,sinit}$ is a skew-symmetric matrix, see eq. (2), consisting of the components of the angular velocity vector of the sensor body frame Ψ^s with respect to the sensor body frame with respect to the initial orientation Ψ^{sinit} , expressed in the sensor body frame Ψ^s .

$$\dot{\mathbf{R}}_s^{sinit} = \mathbf{R}_s^{sinit} \cdot \tilde{\omega}_s^{s,sinit} \quad (1)$$

$$\tilde{\omega}_s^{s,sinit} = \begin{bmatrix} 0 & -\omega_z & \omega_y \\ \omega_z & 0 & -\omega_x \\ -\omega_y & \omega_x & 0 \end{bmatrix} \quad (2)$$

In [12] it is explained that besides the actual rotation value around an axis, the order of the rotation also affects the orientation. The rotations are non-commutative. However when the individual rotations are small enough by minimizing the time step, the order of rotation may be neglected [12]. The sampling frequency must therefore be large enough.

B. Drift analysis

It is shown in earlier work that the offsets and the white noise, sometimes referred to as angle random walk, are usually the most important sources of error [5]. These integrated errors propagate through the strapdown inertial navigation algorithm and increase over time [13]. Drift in the estimated 3D orientation should be minimized as it affects the rotated acceleration too.

A gyroscope can be modelled as (3), where the measured angular velocity $\omega_{s,e}$ is influenced by the the gain g , bias b and stochastic component σ . For an ideal calibrated sensor the gain is correct and the bias and stochastic component are zero, such that the output of the gyroscope is an angular velocity without errors. This will result in a drift-free 3D orientation estimation. Even though with calibrating and subtracting bias b an offset b_e may still be present, as not the complete offset \hat{b} is subtracted, see (4).

$$\omega_{s,e} = g(\omega_s) + b + \sigma \quad (3)$$

$$\hat{b} = b + b_e \quad (4)$$

It is expected that the bias has the largest influence on the drift. The effect of the stochastic component is assumed to be minimal, since the errors result in a drift growing over the square root of time, while the offset grows linearly over time [5]. If the stochastic component is smaller than the offset this expectation holds. The gain is assumed to be correct.

In the situation that the bias is the only major influence on the drift in the orientation estimation, the effect can be analysed. (5) shows the solution of $\dot{\mathbf{R}}$ for the first iteration. The m_c components are constants of the initial rotation matrix. Note that the measured angular velocity consists out of the ideal angular velocity and the error in the offset, $\omega_{e,x} = \omega_x + b_e$. It can be seen that the offset will cause a

drift in the orientation. The magnitude of this drift depends on orientation in each iteration.

$$\dot{\mathbf{R}}_1 = \begin{bmatrix} m_{12}\omega_{e,z} - m_{13}\omega_{e,y} & m_{13}\omega_{e,z} - m_{11}\omega_{e,x} \\ m_{22}\omega_{e,z} - m_{23}\omega_{e,y} & m_{23}\omega_{e,z} - m_{21}\omega_{e,x} \\ m_{32}\omega_{e,z} - m_{33}\omega_{e,y} & m_{33}\omega_{e,z} - m_{31}\omega_{e,x} \\ & m_{11}\omega_{e,y} - m_{12}\omega_{e,x} \\ & m_{21}\omega_{e,y} - m_{22}\omega_{e,x} \\ & m_{31}\omega_{e,y} - m_{32}\omega_{e,x} \end{bmatrix} \quad (5)$$

In the case where only a 1D motion exist, such that the rotation is only about one axis, the orientation can be presented as (6) and (7). Where the angular velocity around the axis is ω_x , $\dot{\mathbf{R}}_i$ the time derivative of (1), n a sample and i the iteration of the time derivative. It is expected that the initial and final orientation of a periodic movement are the same. Since the rotation is only about one axis, it is expected that the offset will be equal to the mean. Similar equations can be achieved with both ω_y and ω_z . The derivations are shown in section V-B.

$$\dot{\mathbf{R}}_i = \begin{bmatrix} 0 & \prod_{n=1}^i (\omega_{x,n} - b_e) & \prod_{n=1}^i (\omega_{x,n} - b_e) \\ 0 & \prod_{n=1}^i (\omega_{x,n} - b_e) & \prod_{n=1}^i (\omega_{x,n} - b_e) \\ 0 & \prod_{n=1}^i (\omega_{x,n} - b_e) & \prod_{n=1}^i (\omega_{x,n} - b_e) \end{bmatrix} \cdot F(i) \quad (6)$$

$$F(i) = \begin{cases} i \cdot \text{mod}(4) = 0 & \begin{bmatrix} 0 & m_{13} & -m_{12} \\ 0 & m_{23} & -m_{22} \\ 0 & m_{33} & -m_{32} \end{bmatrix} \\ i \cdot \text{mod}(4) = 1 & \begin{bmatrix} 0 & -m_{12} & -m_{13} \\ 0 & -m_{22} & -m_{23} \\ 0 & -m_{32} & -m_{33} \end{bmatrix} \\ i \cdot \text{mod}(4) = 2 & \begin{bmatrix} 0 & -m_{13} & m_{12} \\ 0 & -m_{23} & m_{22} \\ 0 & -m_{33} & m_{32} \end{bmatrix} \\ i \cdot \text{mod}(4) = 3 & \begin{bmatrix} 0 & m_{12} & m_{13} \\ 0 & m_{22} & m_{23} \\ 0 & m_{32} & m_{33} \end{bmatrix} \end{cases} \quad (7)$$

C. Drift compensation

Determining the orientation and cancelling the drift will be done by exploiting the cyclical behavior of running. The main idea revolves around the following assumption: If a person is running with a constant speed along a straight line, the cycles and its values should be similar to respectively the other cycles and its values. Therefore in the orientation estimation the same phases in different cycles should estimate the same orientation.

The first method will remove the mean of the angular velocity. The second method rotates the angular velocity to the axis on the knee perpendicular to the sagittal plane. The third method will instead of removing the mean, set a custom offset such that the drift is minimized.

In each method, the signal was truncated to a full number of cycles. Note that a cycle is defined as one whole period of a gait cycle that starts and end with the same event, the

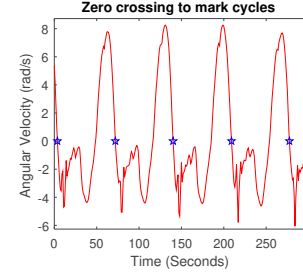


Fig. 3. Marking the cycles of $\omega_{s,y}$ using zero crossing on the falling edge of the signal.

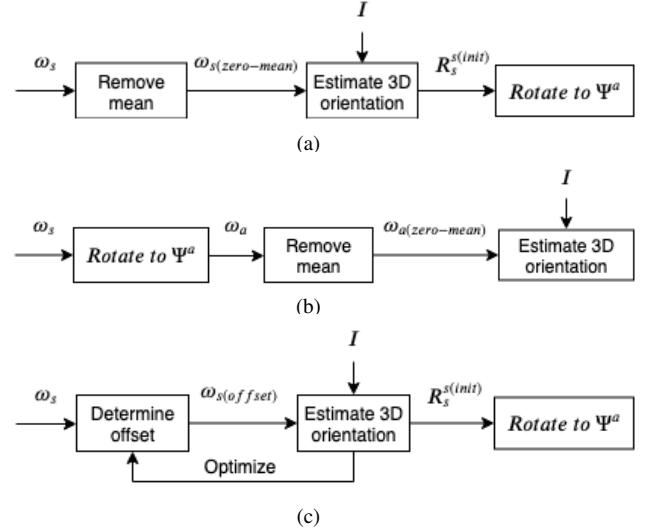


Fig. 4. The approach for each method. (a) shows method 1, (b) shows method 2 and (c) shows method 3.

method should work for any event that is distinguishable in the measured angular velocity data. The axis with the most dominant rotation around the axis on the knee perpendicular to the sagittal plane was used to truncate the signal. This was done by using the zero crossing of the falling edge, this is just before the leg comes in contact with the ground. In this work the axis was $\omega_{s,y}$. Due to the sampling frequency, a sample point with the value zero is not always defined, therefore the closest value is marked as the zero crossing. The marking is shown in Fig. 3.

1) *Method 1: Mean subtraction:* Since each cycle is expected to be very similar, there will be almost no variation between the cycles in the measured data. It is expected that this holds for the estimated orientation too. It is assumed that any bias in the measured data would result in a linear deviation in the orientation. Over a whole number of cycles, the mean of the measured data should therefore be equal to zero. This situation is mathematically described in (5). By subtracting the mean, the linear drift may be removed.

This zero-mean angular velocity $\omega_{s(\text{zero-mean})}$ will be integrated using the differential equation (1) with the identity matrix I as initial orientation to acquire the orientation of the sensor with respect to the initial orientation. To compare this method with the following two methods, the orientation will be rotated with \mathbf{R}_s^a to a partial segment coordinate frame with the same rotation matrix as used in method 2.

2) *Method 2: Rotation to partial segment coordinate frame:* During a measurement the orientation of the sensor is likely not aligned with the segment, due to the need to rigidly attach it to the body, for example in this research on the tibia. Since the orientation estimation itself is non-commutative, errors can arise. By ensuring a small time step, an attempt is made to minimize this effect. It is expected that during running the tibia will mostly rotate around the axis on the knee perpendicular to the sagittal plane. Since each cycle will be similar, the sensor body frame may be rotated to a partial segment coordinate frame, such that most variation of the angular velocity is around one axis. The angular velocity around the other two axes will be smaller. With this method a uni-axial movement is approached, therefore the order of rotation will matter less. It is expected that the rotated angular velocity can be modelled by (6) and the mean can be subtracted to remove the error in the offset b_e .

For the rotation to the partial segment coordinate frame, three axes should be determined to create the rotation matrix \mathbf{R}_s^a . Principal component analysis (PCA) is used to determine the axis on the knee perpendicular to the sagittal plane. PCA is a statistical procedure that can show the relationship between variables by constructing principal components (PC), which are orthogonal and linear combinations [14]. This is done by first subtracting the mean from the data itself. Then a vector is determined which finds the largest possible variance of projections of the data points on that specific vector, this results in PC1. It is assumed that during running the highest variation in angular velocity $\boldsymbol{\omega}_s$ is around the axis on the knee perpendicular to the sagittal plane. By taking a number of complete gait cycles PC1 should resemble this axis.

Two additional axes have to be determined for the construction of the rotation matrix \mathbf{R}_s^a . It may be that there is a variation in drift as the values of two remaining axes differ depending on the rotation. Though it is expected that the results will be similar due to the fact that the majority of the variation in the angular velocity is covered by PC1. This rotation matrix is also used for the other two methods.

For determining the rotation matrix \mathbf{R}_s^a eq. (8) is used. The unit axis y_s is used with PC1 to find a perpendicular third axis. This third axis is used with PC1 to make y_s orthogonal. The three axes are rows in the rotation matrix.

$$\begin{aligned}
 y_s &= [0 \ 1 \ 0] \\
 z_s^a &= PC1 \times y_s \\
 z_s^a &= \frac{z_s^a}{\|z_s^a\|} \\
 y_s^a &= z_s^a \times PC1 \\
 y_s^a &= \frac{y_s^a}{\|y_s^a\|} \\
 \mathbf{R}_s^a &= [PC1; y_s^a; z_s^a]
 \end{aligned} \tag{8}$$

After the signal is rotated, the mean will be subtracted of the angular velocity $\boldsymbol{\omega}_a$ and this result will be integrated in the same manner as in the mean subtraction method by using the differential equation (1) with the identity matrix \mathbf{I} as initial orientation.

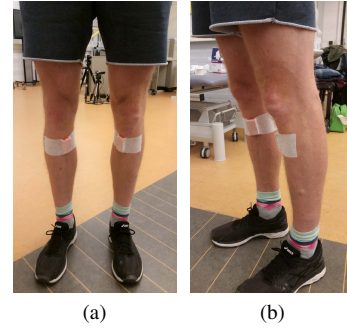


Fig. 5. Placement of the sensors on the tibia's

3) *Method 3: Custom offset:* This method starts with the same reasoning as the mean subtraction method, the expectation is that there should be a minimal variation in the orientation between the cycles in a drift-free estimation. However, instead of using the zero-mean of the angular velocity $\boldsymbol{\omega}_{s(zero-mean)}$, a custom offset is used that subtracts a constant from $\omega_{s,x}$, $\omega_{s,y}$ and $\omega_{s,z}$. This custom offset will be determined with an iterative approach to remove the drift. In the ideal situation, b_e as shown in (4) is subtracted from each of the axes.

After the custom offset has been subtracted, the angular velocity $\boldsymbol{\omega}_{s(offset)}$ will be integrated as done in the mean subtraction method. To compare the results with method 2, the orientation is rotated to the partial segment coordinate frame with the same rotation matrix \mathbf{R}_s^a used in the previous method. The amount of drift is calculated and a new improved custom offset is determined. This is done until an average standard deviation of all cycles of the orientation of less than 2° is found.

D. Participants and measurement setup

The measurements were performed with two healthy male subjects with running experience. With age: 23.5 ± 1.5 , mass: 81.5 ± 11.5 kg and height: 1.88 ± 0.12 m. Both participants were informed about the experimental procedure, the purpose of the acquired data and the risk involved. Both participants signed an informed consent. The measurement was conducted in accordance with the Declaration of Helsinki, and the protocol was approved by the Ethical Committee of the faculty.

The subjects were measured consecutively. Two sensors were placed on the tuberositas tibia of the right and left leg of the first subject, see Fig. 5. The sensors of the left and right tibia were also placed respectively on the left and right tibia of the second subject. The sensors were fixed with double-sided tape between the sensor and the subject's skin and reinforced with additional tape over the sensor onto the leg. This rigid approach was done to minimize the tremors of the sensor itself and ensure that the position of the sensor was fixed. The measurement proceeded as follows:

The subject stands upright for a number of seconds. The subject squats five times, making sure the knees are pointed forward. The subject raises his right leg while supporting his balance by holding on to a bar, next he swings his lower leg back and forth five times. This is repeated with the other leg.

The measurement continues with walking and running on a large treadmill (ForceLink, Culemborg, the Netherlands) for 90 seconds for each speed. The speeds were 4, 6, 10, 12 and 14km/h. Between each walking and running there was a small break to start the next measurement, the subject was asked if he needed rest and if he would like to continue.

1) *Material:* For the measurement wireless inertial sensors (Xsens Technologies B.V., the Netherlands) were used. These were the MTw Awinda of which the unprocessed accelerometer and gyroscope data could be extracted. The sensors were wireless connected with the Awinda Station, ensuring a sample frequency of 100Hz. The MTw sensors had either firmware version 2.0.8 or 2.1.2. The weight of one sensor is 16 gram. The range of the acceleration is $\pm 160m/s^2$, the range of the gyroscope is $\pm 2000deg/s \approx \pm 34.91rad/s$.

E. Method analysis

As mentioned in section II-C, the purpose of the methods is to minimize the drift in the estimation of the 3D orientation.

The analyzation of the results is done using quaternions, to which the rotation matrix of the estimated orientation is converted to. A quaternion can be used as representation of a rotation or an orientation. It is defined as $q = q_0 + \mathbf{q} = q_0 + (i\mathbf{q}_1 + j\mathbf{q}_2 + k\mathbf{q}_3)$. q_0 is referred to as the scalar part, whereas the \mathbf{q} is the vectorial part [16]. With q_0 , the magnitude of the rotation between the initial orientation and another orientation can be shown. Whereas $q_0 = 1$ means there is no orientation difference and $q_0 = 0$ indicates a rotation of 180° [17]. Since the initial orientation is just before the impact of the leg on the ground, it is expected that without drift in each cycle the scalar is between 0 and 1.

The amount of drift will be represented by the average of the standard deviation of all samples in the cycles. A lesser drift would result in a lower average standard deviation, as it is expected that the orientation in each phase of the cycle will be nearly the same.

Note that the quaternion representation is solely used for determining the drift in the orientation.

For the custom offset method, the offset was determined manually, however the optimization process can be done automatically. The data was analyzed offline in MatLab R2016b.

III. RESULTS

First important aspects of the measurement data are show. Then the results are in order of the presented drift cancellation methods. Note that only the data of subject 1 while running 12km/h is displayed in the figures, the results are representative for both the other speeds and for subject 2. Besides that only the data of the sensor on the right tibia was processed.

The gyroscope is subdue to noise, while stationary on a flat surface the standard deviation is 0.0048, 0.0051 and 0.0050 rad/s for respectively $\omega_{s,x}$, $\omega_{s,y}$ and $\omega_{s,z}$.

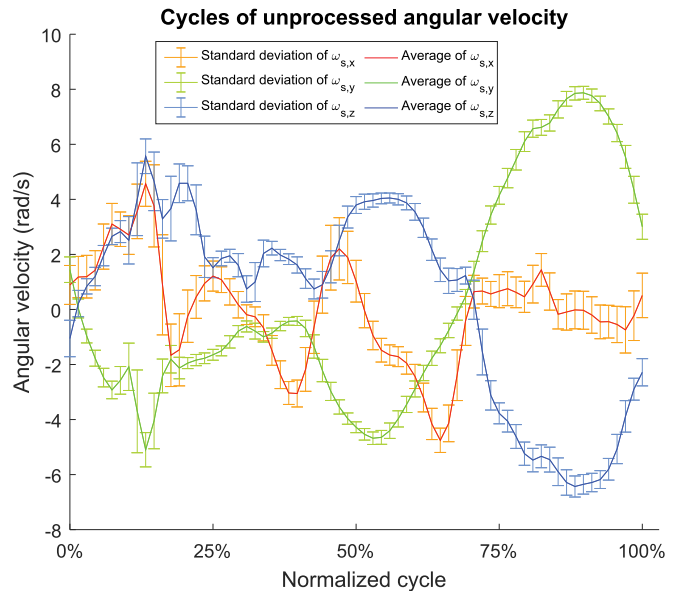


Fig. 6. The mean and standard deviation of all samples in each cycle of each axis of unprocessed angular velocity ω_s in rad/s in the sensor body frame Ψ^s .

Axis\Speed	10km/h	12km/h	14km/h
Average standard deviation of $\omega_{s,x}$ (rad/s)	0.7079	0.7000	0.8748
Average standard deviation of $\omega_{s,y}$ (rad/s)	0.3399	0.3357	0.4486
Average standard deviation of $\omega_{s,z}$ (rad/s)	0.4727	0.4675	0.5776

TABLE I

THE AVERAGE STANDARD DEVIATION OF ALL SAMPLES IN EACH CYCLE OF EACH AXIS OF ω_s IN RAD/S FOR SUBJECT 1.

Axis\Speed	10km/h	12km/h	14km/h
Average standard deviation of $\omega_{s,x}$ (rad/s)	0.6743	0.7679	0.9848
Average standard deviation of $\omega_{s,y}$ (rad/s)	0.2479	0.3307	0.4988
Average standard deviation of $\omega_{s,z}$ (rad/s)	0.3437	0.4531	0.5946

TABLE II

THE AVERAGE STANDARD DEVIATION OF ALL SAMPLES IN EACH CYCLE OF EACH AXIS OF ω_s IN RAD/S FOR SUBJECT 2.

The unprocessed angular velocity ω_s can be seen in Fig. 6, were all the cycles have a normalized length. The mean and standard deviation in each part of the cycle are plotted. The number of cycles for subject 1 at 12km/h is 140. There appears to be more variation at changes in the angular velocity. Table I and II show the average standard deviation of all samples of in each cycle of each axis of ω_s for subject 1 and 2.

Fig. 7 shows the scalar of the quaternions of the orientation estimation over the number of samples for without any drift compensation in Fig. 7a and each of the drift compensation methods. Fig. 7d and 7c show a zoom of the first and last part of the measurement, to indicate the cyclic behaviour and its differences over time. Note that Fig. 7c shows the scalar of the quaternions of method 2, however without the mean subtraction before the 3D orientation estimation. It appeared that the with the mean subtraction, method 2 produced similar heavily drift results to method 1. The offsets of the custom offset method are in Table III and IV.

Fig. 8 shows the mean and standard deviation of all samples in each cycle of q_1 , q_2 and q_3 of the estimated

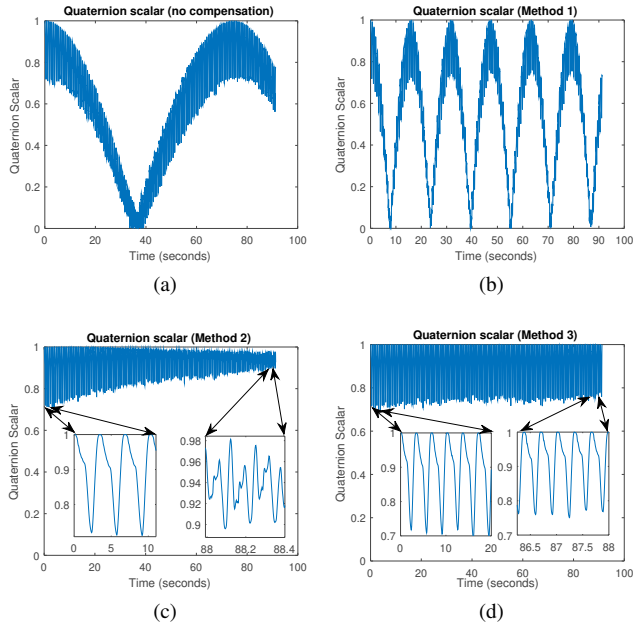


Fig. 7. The scalar of the quaternions of the 3D orientation estimation over time in seconds for (a) no compensation, (b) method 1: mean subtraction, (c) method 2: rotation to partial segment, however without the mean subtraction and (d) method 3: custom offset are visualized.

Axis/Speed	4km/h	6km/h	10km/h	12km/h	14km/h
$\omega_{s,x}$	0.0500	0.0470	0.0740	0.0935	0.1185
$\omega_{s,y}$	-0.0050	0.0020	-0.0030	-0.0048	-0.0023
$\omega_{s,z}$	-0.0015	-0.0065	-0.0060	-0.0049	-0.0004

TABLE III
OFFSETS USED FOR THE ANGULAR VELOCITY ω_s IN RAD/S FOR THE CUSTOM OFFSET METHOD FOR SUBJECT 1.

Axis/Speed	4km/h	6km/h	10km/h	12km/h	14km/h
$\omega_{s,x}$	0.0275	0.0380	0.0650	0.0940	0.1200
$\omega_{s,y}$	-0.0018	-0.0055	-0.0080	-0.0110	-0.0080
$\omega_{s,z}$	-0.0110	-0.0148	-0.0160	-0.0150	-0.0105

TABLE IV
OFFSETS USED FOR THE ANGULAR VELOCITY ω_s IN RAD/S FOR THE CUSTOM OFFSET METHOD FOR SUBJECT 2.

3D orientation. This is for the orientation without drift compensation in Fig. 8b, method 1 in Fig. 8a, method 2 without the mean subtraction in Fig. 8c, method 3 in Fig. 8d and method 2 with a custom offset in Fig. 8e.

IV. DISCUSSION

A. Measured data

As seen in Fig. 6, where the mean and standard deviation of all the cycles of each axis are plotted, the measured angular velocity ω_s is cyclical. Both the y and z axes seem to have a large component of the rotation around the axis perpendicular on the sagittal plane. This is as expected as the sensors were not placed such that the sensor was in a forward direction, but on the flat part of the upper tibia facing inward, as shown in Fig. 5.

The average and the average standard deviation over all cycles of the unprocessed angular velocity is shown in Table I for subject 1 and Table II for subject 2. The variation in the cycles may be caused by a slight variation in the

walking or running pattern. Since the methods are based on the cyclical behaviour, there is a limit to the accuracy the methods can achieve if the running pattern deviates from cyclical behaviour. The noise of the gyroscope is two orders of magnitude smaller than the standard deviation of the cycles. Therefore the noise does not influence the methods significantly, as expected in section II-B.

B. No compensation

The estimated 3D orientation without any compensation for the drift shows a strong drift, as shown in Fig. 7a. For both subjects it has been observed that the drift increases slightly at 14km/h and decreases slightly at 10km/h, with respect to 12km/h. This is likely due to the fact that a higher speed has a higher number of cycles during the 90 seconds of the measurement. The higher number of cycles leads to more variation in the orientation and therefore more drift.

C. Method 1: Mean subtraction

The mean subtraction method seems not to be able to reduce the drift, as shown in Fig. 7b. In fact, the drift is larger than without a compensation. This shows that when the dominant rotation in the signal is present in at least two axes, the mean in the angular velocity does not resemble the extra offset b_e .

D. Method 2: Rotation to partial segment coordinate frame

The mean subtraction after the rotation to partial segment coordinate frame does not seem to work either. It gave a similar result as method 1, Fig. 7b. However, the drift is significantly reduced without the mean subtraction, shown in Fig. 7c. Although the 3D orientation was still affected by the minor rotations of the other two axes, the mean subtraction seems not to resemble the extra offset b_e in a 1D dominant situation.

It can be seen in Fig. 7c that the drift increases over time. This is emphasized by the large standard deviation showed in Fig. 8c.

For this method it was noticed that besides the PC1 as x-axis in the partial segment coordinate system, the other two orthogonal axes significantly influenced the amount of drift. Instead of the chosen unit axis $y_s = [0 \ 1 \ 0]$, unit axis $[0.5571 \ 0.3714 \ 0.7428]$ was used which showed much less drift. Remarkably, when the PCA was taken as rotation matrix the estimated orientation showed an amount of drift comparably to the amount of drift with no drift compensation at all. This suggests that this method might be optimized besides the use of a custom offset as mentioned earlier.

It was noted that the determined z-axis and corrected y-axis in the rotation to Ψ^a for subject 2 was approximately 180° turned with respect to subject 1.

E. Method 3: Custom offset

With the custom offset method the drift is minimized by manual optimization for both walking and running. The offsets can be seen in Table III and Table IV for subject 1 and 2. It seems that higher velocities need a higher offset in $\omega_{s,x}$, though the offsets of $\omega_{s,y}$ and $\omega_{s,z}$ do not show such a clear consistent relation.

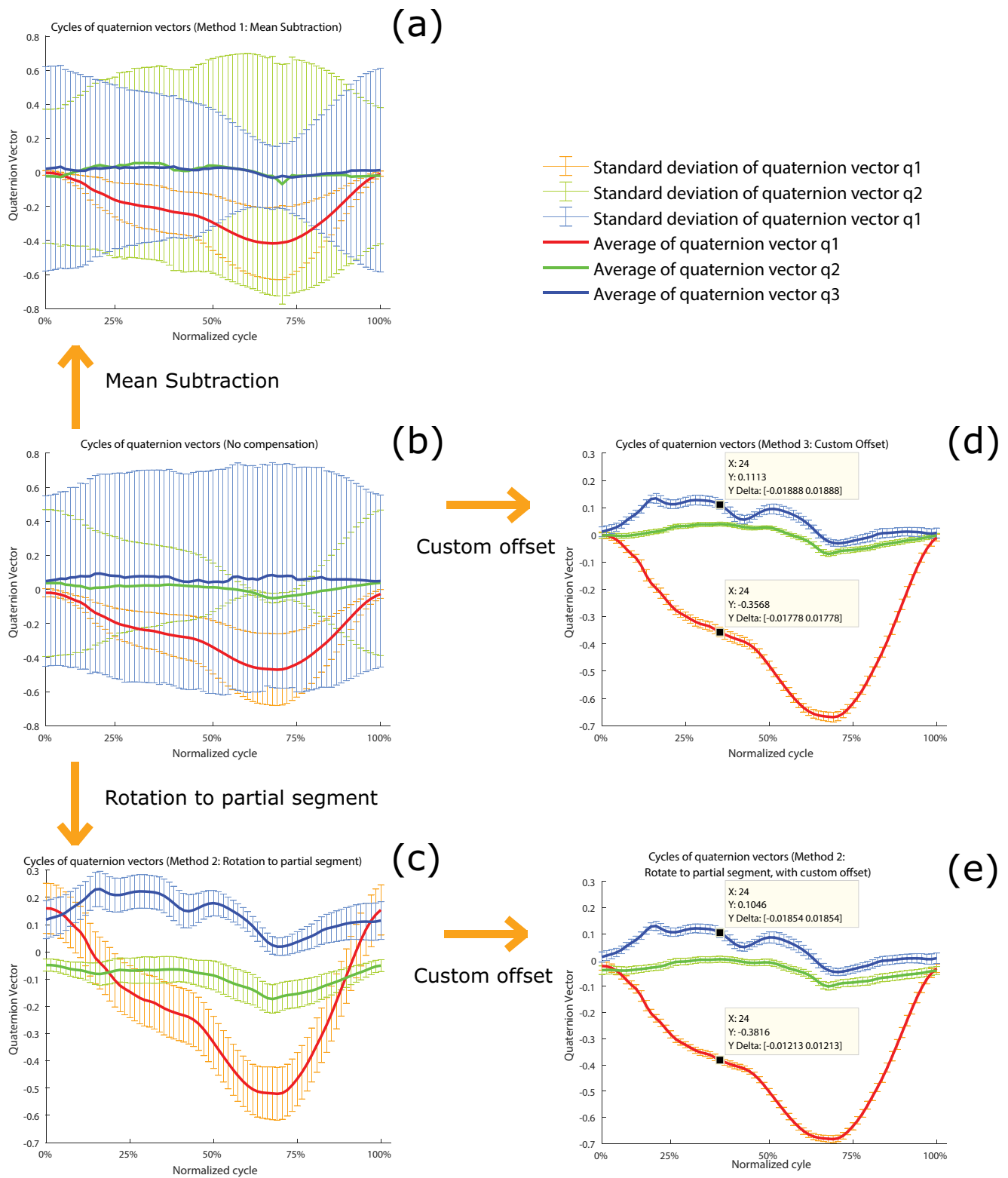


Fig. 8. The average and standard deviation of all samples in each cycle with normalized length of q_1 , q_2 and q_3 of the estimated 3D orientation. The estimated 3D orientation without any compensation is shown in (b). Method 1 is shown in (a), method 2 without mean subtraction is shown in (c) and method 3 is shown in (d). (e) shows method 2 with a custom offset. Note that (d) is optimized to a lower average standard deviation.

Speed (km/h)	q_1	q_2	q_3	Average standard deviation
4	-0.3036 (0.0183)	0.0801 (0.0413)	-0.3116 (0.2015)	0.0870
6	-0.3250 (0.0068)	0.0249 (0.0045)	0.0002 (0.0155)	0.0089
10	-0.3297 (0.0120)	-0.0216 (0.0111)	0.0407 (0.0142)	0.0124
12	-0.3550 (0.0164)	-0.0036 (0.0087)	0.0525 (0.0160)	0.0137
14	-0.3610 (0.0167)	0.0376 (0.0128)	0.0220 (0.0212)	0.0169

TABLE V

AVERAGE, STANDARD DEVIATION AND AVERAGE STANDARD DEVIATION OF THE QUATERNIONS q_1 , q_2 AND q_3 FOR SUBJECT 1 USING THE OFFSETS IN TABLE III.

Speed (km/h)	q_1	q_2	q_3	Average standard deviation
4	0.3088 (0.0235)	0.0245 (0.0060)	-0.0107 (0.0211)	0.0169
6	0.3530 (0.0098)	0.0152 (0.0058)	-0.0309 (0.0169)	0.0108
10	0.3872 (0.0188)	0.0141 (0.0134)	-0.0399 (0.0160)	0.0161
12	0.4323 (0.0151)	0.0144 (0.0118)	-0.0143 (0.0201)	0.0157
14	0.4524 (0.0200)	0.0514 (0.0241)	-0.0373 (0.0244)	0.0228

TABLE VI

AVERAGE, STANDARD DEVIATION AND AVERAGE STANDARD DEVIATION OF THE QUATERNIONS q_1 , q_2 AND q_3 FOR SUBJECT 2 USING THE OFFSETS IN TABLE IV.

In Fig. 7d it can be seen that the scalar of the quaternion is repetitive and does approach the value 1 in each cycle, meaning that the orientation is almost the same to the initial orientation. Though, over the number of samples the scalar decreases slightly in variation. This means that the variation from the initial orientation is less. This might be due to a drift that is not compensated for, such as a non-ideal custom offset, a bias that changes over time or integrated white noise. Another assumption is that the actual running differed over time, where the lower leg may had a smaller extension during the strides. In the zoom of the initial and last part the scalar shows the same behaviour except for the amplitude, the most likely reasoning therefore is the changing running pattern. In addition to that at 10km/h the orientation during running has a lower variation, while at 14km/h there is a larger variation.

Fig. 8d shows that the custom offset performs better than method 1 and 2. The average and standard deviation of all samples in each cycle of q_1 , q_2 and q_3 are shown. For most cases, the average standard deviation can be optimized below 0.017, which translates to approximately 2 degrees for each axis in Euler Angles.

The estimated 3D orientation of subject 2 at 14km/h was subject to a non-linear drift in q_2 and q_3 , a second-order behaviour was noticed. It might be that the runner shifted his orientation slightly during the running back and forth. Another cause may be an instability of the offset which may change over time. A constant offset over the whole running period can not compensate for this. The estimated 3D orientation of subject 1 at 4km/h shows a relative large standard deviation, though the drift seemed linear more optimized offsets were not found.

On the contrary of the mean subtraction in method 2, a custom offset was used instead and the drift compensation showed similar results as method 3. This is shown in Fig. 8e. It was noticed that, to achieve an average standard deviation below 2 degrees, the required offsets of $\omega_{a,x}$ were significantly lower than for method 3, as shown in Table VII.

Subject/Speed	10km/h	12km/h	14km/h
Subject 1	0.0080	0.0080	0.0070
Subject 2	-0.0100	-0.0100	-0.0125

TABLE VII

OFFSETS USED FOR THE ANGULAR VELOCITY $\omega_{a,x}$ IN RAD/S FOR METHOD 2 WITH CUSTOM OFFSET.

F. Limitations and recommendations

Method 2 shows that in a signal with a 1D dominant rotation the drift can be reduced by rotating one axis such that the dominant rotation is around this axis. Though it was found that the rotation of the other two axes mattered. The method may therefore be optimized.

The custom offset method only applies for a bias which causes linear deviations. Drift caused by white noise is not directly accounted for, neither is drift that is non-linear and time dependent.

The current method with custom offset is not yet robust to changes in the running pattern. The method has only been tested for a constant speed, as each constant speed required a unique offset. A varying speed would not likely work with the constant custom offsets. Besides that, it is assumed that the subject is running in a straight line without turns or running up and down a certain gradient.

The methods are only tested for the sensor on the right tibia. Since it is based on the cyclical nature of running, it is expected that method 2 with a custom offset and method 3 work for the left tibia too. For other body parts where a cyclical behaviour is present method 3 is expected to work too. Method 2 with a custom offset might work as well, though this depends on the rotation of the body part. This has to be verified.

V. CONCLUSION

This work shows that exploiting the cyclical behaviour of running can help to reduce the drift when the orientation is estimated. The same phases in different cycles have a similar estimate of the 3D orientation. A custom offset, for both method 2 as for method 3, delivers the best results. An accuracy of at least 2 degrees can be achieved for both walking and running.

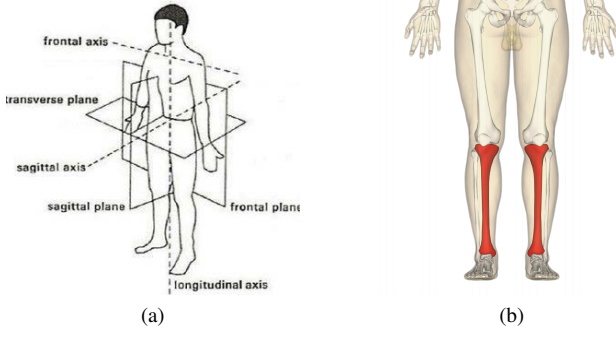


Fig. 9. (a) Anatomical planes of the human body. Source: [18]. (b) Location of the tibia (red) in the human body. Source: [19]

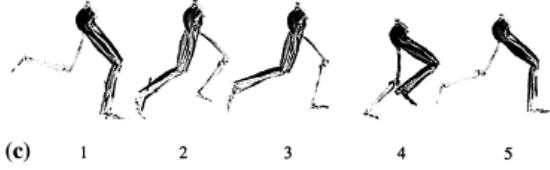


Fig. 10. Running phases: 1. Stance phase absorption. 2. Stance phase generation. 3. Swing phase generation. 4. Swing phase reversal. 5. Swing phase absorption. Source: [20]

APPENDIX

A. The human body

The human body can be divided into three orthogonal planes, in this paper they are referred to as the frontal plane, the transverse plane and the sagittal plane. See Fig. 9a. The direction of forward movement is perpendicular to the frontal plane, towards the front of the body.

As mentioned in the introduction, a minimal set of three sensors is chosen to identify and detect risks during running. In this research the method is only applied on the motions of the tibia, see Fig. 9b and 5. It is expected that during running the most variance in angular velocity of the tibia, is around the axis on the knee perpendicular to the sagittal plane. It is assumed that when a person stands straight, the tibia is aligned perpendicular to the transverse plane.

During running, several phases in the gait cycle can be differentiated, as pictured in Fig. 10. It is important to identify these phases in the measurement data to distinguish each running cycle. It is expected that between the swing phase absorption (5) and the stance phase absorption (1) a peak will be measured by the accelerometer due to the impact of the leg hitting the ground. It is expected that the gyroscope measures a peak during the swing phase, depicted as 3 in the figure.

B. Derivation drift analysis

This section shows the derivation of equations (5), (6) and (7). The differential equation for the 3D orientation estimation is:

$$\dot{\mathbf{R}}_s^{S_{init}} = \mathbf{R}_s^{S_{init}} \cdot \tilde{\boldsymbol{\omega}}_s^{S_{init}} \quad (9)$$

$$(10)$$

Where $\tilde{\boldsymbol{\omega}}_s^{S_{init}}$ is the skew-symmetric matrix:

$$\tilde{\boldsymbol{\omega}}_s^{S_{init}} = \begin{bmatrix} 0 & -\omega_z & \omega_y \\ \omega_z & 0 & -\omega_x \\ -\omega_y & \omega_x & 0 \end{bmatrix} \quad (11)$$

The meaning of (11) and (9) are explained in Section II-A. For the following derivations the notation of the reference frame is omitted. Equation (5) is the result of the first iteration of the following matrix multiplication with an initial rotation matrix. The measured angular velocity consists out of the ideal angular velocity and the error in the offset, $\omega_{e,x} = \omega_x + b_e$. Note that since the derivation is only one iteration of the differential equation, the unique angular velocities for every iteration are omitted for this derivation.

$$\dot{\mathbf{R}}_1 = \begin{bmatrix} m_{11} & m_{12} & m_{13} \\ m_{21} & m_{22} & m_{23} \\ m_{31} & m_{32} & m_{33} \end{bmatrix} \cdot \begin{bmatrix} 0 & -\omega_{e,z} & \omega_{e,y} \\ \omega_{e,z} & 0 & -\omega_{e,x} \\ -\omega_{e,y} & \omega_{e,x} & 0 \end{bmatrix} \quad (12)$$

$$\dot{\mathbf{R}}_1 = \begin{bmatrix} m_{12}\omega_{e,z} - m_{13}\omega_{e,y} & m_{13}\omega_{e,z} - m_{11}\omega_{e,x} \\ m_{22}\omega_{e,z} - m_{23}\omega_{e,y} & m_{23}\omega_{e,z} - m_{21}\omega_{e,x} \\ m_{32}\omega_{e,z} - m_{33}\omega_{e,y} & m_{33}\omega_{e,z} - m_{31}\omega_{e,x} \\ m_{11}\omega_{e,y} - m_{12}\omega_{e,x} \\ m_{21}\omega_{e,y} - m_{22}\omega_{e,x} \\ m_{31}\omega_{e,y} - m_{32}\omega_{e,x} \end{bmatrix} \quad (13)$$

In equation (6) and (7) only a 1D rotation about one axis exists. For this derivation the axis is the x-axis, but the derivation is similar for the other two axes. This results in the following matrix multiplications:

$$\dot{\mathbf{R}}_1 = \begin{bmatrix} m_{11} & m_{12} & m_{13} \\ m_{21} & m_{22} & m_{23} \\ m_{31} & m_{32} & m_{33} \end{bmatrix} \cdot \begin{bmatrix} 0 & 0 & 0 \\ 0 & 0 & -\omega_{e,x,1} \\ 0 & \omega_{e,x,1} & 0 \end{bmatrix} \quad (14)$$

$$\dot{\mathbf{R}}_2 = \begin{bmatrix} 0 & m_{13}\omega_{e,x_1} & -m_{12}\omega_{e,x_1} \\ 0 & m_{23}\omega_{e,x_1} & -m_{22}\omega_{e,x_1} \\ 0 & m_{33}\omega_{e,x_1} & -m_{32}\omega_{e,x_1} \end{bmatrix} \cdot \begin{bmatrix} 0 & 0 & 0 \\ 0 & 0 & -\omega_{e,x,2} \\ 0 & \omega_{e,x,2} & 0 \end{bmatrix} \quad (15)$$

$$\dot{\mathbf{R}}_3 = \begin{bmatrix} 0 & -m_{12}\omega_{e,x_1}\omega_{e,x_2} & -m_{13}\omega_{e,x_1}\omega_{e,x_2} \\ 0 & -m_{22}\omega_{e,x_1}\omega_{e,x_2} & -m_{23}\omega_{e,x_1}\omega_{e,x_2} \\ 0 & -m_{32}\omega_{e,x_1}\omega_{e,x_2} & -m_{33}\omega_{e,x_1}\omega_{e,x_2} \\ 0 & 0 & 0 \\ 0 & 0 & -\omega_{e,x,3} \\ 0 & \omega_{e,x,3} & 0 \end{bmatrix} \quad (16)$$

A pattern exists, as the first column of $\dot{\mathbf{R}}_i$ is always 0 and the constant of the initial rotation matrix is alternating between the second and third column. The signs of the columns are switched every two iterations. With this knowledge the product of the unique angular velocities and the signs and constants of the initial rotation matrix can be generalized.

$$\dot{\mathbf{R}}_i = \begin{bmatrix} 0 & \prod_{n=1}^i (\omega_{x,n} - b_e) & \prod_{n=1}^i (\omega_{x,n} - b_e) \\ 0 & \prod_{n=1}^i (\omega_{x,n} - b_e) & \prod_{n=1}^i (\omega_{x,n} - b_e) \\ 0 & \prod_{n=1}^i (\omega_{x,n} - b_e) & \prod_{n=1}^i (\omega_{x,n} - b_e) \end{bmatrix} \cdot F(i) \quad (17)$$

$$F(i) = \begin{cases} i \cdot \text{mod}(4) = 0 & \begin{bmatrix} 0 & m_{13} & -m_{12} \\ 0 & m_{23} & -m_{22} \\ 0 & m_{33} & -m_{32} \end{bmatrix} \\ i \cdot \text{mod}(4) = 1 & \begin{bmatrix} 0 & -m_{12} & -m_{13} \\ 0 & -m_{22} & -m_{23} \\ 0 & -m_{32} & -m_{33} \end{bmatrix} \\ i \cdot \text{mod}(4) = 2 & \begin{bmatrix} 0 & -m_{13} & m_{12} \\ 0 & -m_{23} & m_{22} \\ 0 & -m_{33} & m_{32} \end{bmatrix} \\ i \cdot \text{mod}(4) = 3 & \begin{bmatrix} 0 & m_{12} & m_{13} \\ 0 & m_{22} & m_{23} \\ 0 & m_{32} & m_{33} \end{bmatrix} \end{cases} \quad (18)$$

ACKNOWLEDGMENT

I would like to thank my daily supervisor Prof.Dr.Ir. Peter Veltink for his readiness to help and his numerous insights on the theory and intermediate results.

Also I would like to thank my secondary supervisor MSc. Marit Zandbergen for her insights on biomechanical subjects and her extensive support during the experimental measurements.

Besides them I would like to express my thanks to my peers for the support during the assignment, the peer reviewing and the participation in the experimental measurements.

REFERENCES

- [1] W. van Mechelen "Running Injuries", *Sports Medicine*, vol. 14, pp. 320, 1992.
- [2] S.L. James "Running Injuries to the Knee", *JAAOS - Journal of the American Academy of Orthopaedic Surgeons*, vol. 3, no. 6, pp. 309-318, 1995.
- [3] Y. Enomoto, T. Aibara and K. Sugimoto "Estimation of the centre of mass and pelvis movement in running using an inertia sensor mounted on sacrum", 2017
- [4] M. Schepers, "Ambulatory Assessment of Human Body Kinematics and Kinetics", Ph.D. thesis, Faculty of Elect. Eng., Math. and Comp. Scn., University of Twente, Enschede, 2009.
- [5] O.J. Woodman, "An introduction to inertial navigation", 2007
- [6] W. T. Latt, K. C. Veluvolu and W. T. Ang "Drift-Free Position Estimation of Periodic or Quasi-Periodic Motion Using Inertial Sensors", 2011.
- [7] X. Yun, E. R. Bachmann and H. Moore "Self-contained Position Tracking of Human Movement Using Small Inertial/Magnetic Sensor Modules", *Proceedings 2007 IEEE International Conference on Robotics and Automation*, 2007.
- [8] S. K. Park and Y. S. Suh "A Zero Velocity Detection Algorithm Using Inertial Sensors for Pedestrian Navigation Systems", 2010.
- [9] M. Ma, Q. Song and Y. Gu "An Adaptive Zero Velocity Detection Algorithm Based on Multi-Sensor Fusion for a Pedestrian Navigation System", 2018.
- [10] V. Bonnet, C. Mazzà and J. McCamley "Use of weighted Fourier linear combiner filters to estimate lower trunk 3D orientation from gyroscope sensors data", 2013
- [11] J.E. Bortz, "A New Mathematical Formulation for Strapdown Inertial Navigation", *IEEE Transactions on Aerospace and Electronic Systems*, vol. 7, no. 1, pp. 61-66, 1971.

- [12] D. H. Titterton and J. L. Weston, *Strapdown Inertial Navigation Technology - 2nd Edition*. IET, 2004, pp. 36-40.
- [13] A. Luttwak, "Human Motion Tracking and Orientation Estimation using inertial sensors and RSSI measurements", Ph.D. thesis, School of Eng. and Comp. Sci., The Hebrew University of Jerusalem, 2011, pp.17-18
- [14] MathWorks, "Principal Component Analysis (PCA)" [Online]. Available: mathworks.com/help/stats/principal-component-analysis-pca.html [Accessed: Oct. 22, 2019]
- [15] M. Paulich, M. Schepers and N. Rudigkeit, "Xsens MTw Awinda: Miniature Wireless Inertial-Magnetic Motion Tracker for Highly Accurate 3D Kinematic Applications", Xsens Technologies B.V., 2018
- [16] J. B. Kuipers, *Quaternions and rotation sequences*. Princeton University Press, Fifth printing, 2002.
- [17] F. van der Heijden, "Math for computer vision and navigation", University of Twente, 2018.
- [18] T. Poluyi, "Control System Development for Six Degree of Freedom Spine Simulator", 2014. Available: https://www.researchgate.net/figure/Anatomical-planes-of-the-upper-region-of-the-human-body-1_fig1_270340667. [Accessed: Nov. 3, 2019]
- [19] Anatomography, "File:Tibia - frontal view.png", *commons.wikimedia.org*, 16 February 2013. Available: commons.wikimedia.org/w/index.php?curid=24693053. [Accessed: Oct. 2, 2019]
- [20] T.F. Novacheck, "The biomechanics of running", *Gait & Posture*, vol. 7, no. 1, pp. 77-95, 1998.
- [21] H.Kortier, "Assessment of Hand Kinematics and Interactions with the Environment", Ph.D. thesis, Faculty of Elect. Eng., Math. and Comp. Sci., University of Twente, Enschede, 2018.
- [22] M. Kok, J.D. Hol and T.B. Schön, "Using Inertial Sensors for Position and Orientation Estimation", *Foundations and Trends in Signal Processing*, vol. 11, no. 1-2, pp. 1-153, 2017 <http://dx.doi.org/10.1561/20000000094>

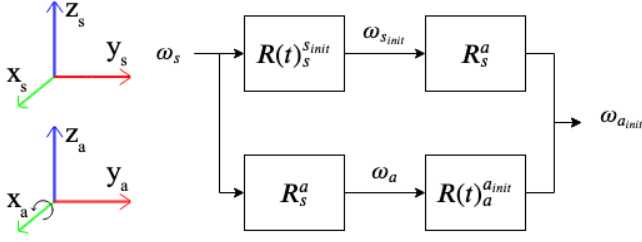


Fig. 2. The sensor body frame Ψ^s with angular velocity ω_s is aligned with the sensor body. The 3D orientation can be estimated with the use of eq. (1). By using this time dependent rotation matrix, the angular velocity $\omega_{s,init}$ with respect to the initial orientation can be calculated. ω_s may be rotated first to the partial segment frame Ψ^a , such that the axis x_a resembles with the axis on the knee perpendicular to the sagittal plane. In a drift-free estimated 3D orientation $\omega_{a,init}$ is identical for both approaches

phase. This method is less suitable for running at higher velocities, as the stance phase is too short [7], [8], [9]. In some work periodic movements are exploited for analytical integration using adaptive filtering methods, such as the weighted-frequency Fourier linear combiner (WFLC) or the band-limited multiple Fourier linear combiner (BMFLC). The measured signals can be modelled with these filters and analytically integrated with the Fourier series. Both are not verified for running [6], [10].

To the best of the author's knowledge, there currently does not seem to be a solution for the drift-free 3D orientation estimation for periodic movements with a single IMU. Therefore a new method in drift cancellation is required. In this research three new methods of drift cancellation are proposed by exploiting the cyclical nature of running. The main idea revolves around the following assumption: If a person is running with a constant speed along a straight line, the gait cycles and its values should be similar to respectively the other gait cycles and its values. With such a method sensors can operate individually on any position on the body during running without the need of extensive calibration beforehand. This work focuses on the drift-free estimation of 3D orientations.

This leads to the research question: How can the cyclical nature of running be used to acquire drift-free estimates of the 3D orientation using a single inertial sensor?

II. METHOD

This section will provide the necessary theory and present the methods to cancel the drift with the use of the cyclic behavior. First, the theory about the estimation of the 3D orientation is given in Section II-A. Analysis of the influence of bias on the drift is shown in II-B. The three methods for drift compensation using cyclical behaviour are proposed in Section II-C. Information about the experimental measurement is elaborated on in Section II-D and finally the analysis of the results is explained in Section II-E.

A. Orientation and integration

The orientation estimation of the sensor body frame Ψ^s depends on previous rotations, as the rotation from the sensor body frame Ψ^s to the sensor body frame with respect to the initial orientation $\Psi^{s,init}$ is time dependent. Therefore the

rotation is done with an adaptation to the differential equation expressed in eq. (1) [11].

The time dependent rotation matrix $\mathbf{R}_s^{s,init}$ expresses the rotation from the sensor body frame Ψ^s to the sensor body frame with respect to the initial orientation $\Psi^{s,init}$. $\dot{\mathbf{R}}_s^{s,init}$ is the time derivative of $\mathbf{R}_s^{s,init}$. $\tilde{\omega}_s^{s,init}$ is a skew-symmetric matrix, see eq. (2), consisting of the components of the angular velocity vector of the sensor body frame Ψ^s with respect to the sensor body frame with respect to the initial orientation $\Psi^{s,init}$, expressed in the sensor body frame Ψ^s .

$$\dot{\mathbf{R}}_s^{s,init} = \mathbf{R}_s^{s,init} \cdot \tilde{\omega}_s^{s,init} \quad (1)$$

$$\tilde{\omega}_s^{s,init} = \begin{bmatrix} 0 & -\omega_z & \omega_y \\ \omega_z & 0 & -\omega_x \\ -\omega_y & \omega_x & 0 \end{bmatrix} \quad (2)$$

In [12] it is explained that besides the actual rotation value around an axis, the order of the rotation also affects the orientation. The rotations are non-commutative. However when the individual rotations are small enough by minimizing the time step, the order of rotation may be neglected [12]. The sampling frequency must therefore be large enough.

B. Drift analysis

It is shown in earlier work that the offsets and the white noise, sometimes referred to as angle random walk, are usually the most important sources of error [5]. These integrated errors propagate through the strapdown inertial navigation algorithm and increase over time [13]. Drift in the estimated 3D orientation should be minimized as it affects the rotated acceleration too.

A gyroscope can be modelled as (3), where the measured angular velocity $\omega_{s,e}$ is influenced by the gain g , bias b and stochastic component σ . For an ideal calibrated sensor the gain is correct and the bias and stochastic component are zero, such that the output of the gyroscope is an angular velocity without errors. This will result in a drift-free 3D orientation estimation. Even though with calibrating and subtracting bias b an offset b_e may still be present, as not the complete offset \hat{b} is subtracted, see (4).

$$\omega_{s,e} = g(\omega_s) + b + \sigma \quad (3)$$

$$\hat{b} = b + b_e \quad (4)$$

It is expected that the bias has the largest influence on the drift. The effect of the stochastic component is assumed to be minimal, since the errors result in a drift growing over the square root of time, while the offset grows linearly over time [5]. If the stochastic component is smaller than the offset this expectation holds. The gain is assumed to be correct.

In the situation that the bias is the only major influence on the drift in the orientation estimation, the effect can be analysed. (5) shows the solution of $\dot{\mathbf{R}}$ for the first iteration. The m_c components are constants of the initial rotation matrix. Note that the measured angular velocity consists out of the ideal angular velocity and the error in the offset, $\omega_{e,x} = \omega_x + b_e$. It can be seen that the offset will cause a

drift in the orientation. The magnitude of this drift depends on orientation in each iteration.

$$\dot{\mathbf{R}}_1 = \begin{bmatrix} m_{12}\omega_{e,z} - m_{13}\omega_{e,y} & m_{13}\omega_{e,z} - m_{11}\omega_{e,x} \\ m_{22}\omega_{e,z} - m_{23}\omega_{e,y} & m_{23}\omega_{e,z} - m_{21}\omega_{e,x} \\ m_{32}\omega_{e,z} - m_{33}\omega_{e,y} & m_{33}\omega_{e,z} - m_{31}\omega_{e,x} \\ m_{11}\omega_{e,y} - m_{12}\omega_{e,x} \\ m_{21}\omega_{e,y} - m_{22}\omega_{e,x} \\ m_{31}\omega_{e,y} - m_{32}\omega_{e,x} \end{bmatrix} \quad (5)$$

In the case where only a 1D motion exist, such that the rotation is only about one axis, the orientation can be presented as (6) and (7). Where the angular velocity around the axis is ω_x , $\dot{\mathbf{R}}_i$ the time derivative of (1), n a sample and i the iteration of the time derivative. It is expected that the initial and final orientation of a periodic movement are the same. Since the rotation is only about one axis, it is expected that the offset will be equal to the mean. Similar equations can be achieved with both ω_y and ω_z . The derivations are shown in section V-B.

$$\dot{\mathbf{R}}_i = \begin{bmatrix} 0 & \prod_{n=1}^i (\omega_{x,n} - b_e) & \prod_{n=1}^i (\omega_{x,n} - b_e) \\ 0 & \prod_{n=1}^i (\omega_{x,n} - b_e) & \prod_{n=1}^i (\omega_{x,n} - b_e) \\ 0 & \prod_{n=1}^i (\omega_{x,n} - b_e) & \prod_{n=1}^i (\omega_{x,n} - b_e) \end{bmatrix} \cdot F(i) \quad (6)$$

$$F(i) = \begin{cases} i \cdot \text{mod}(4) = 0 & \begin{bmatrix} 0 & m_{13} & -m_{12} \\ 0 & m_{23} & -m_{22} \\ 0 & m_{33} & -m_{32} \end{bmatrix} \\ i \cdot \text{mod}(4) = 1 & \begin{bmatrix} 0 & -m_{12} & -m_{13} \\ 0 & -m_{22} & -m_{23} \\ 0 & -m_{32} & -m_{33} \end{bmatrix} \\ i \cdot \text{mod}(4) = 2 & \begin{bmatrix} 0 & -m_{13} & m_{12} \\ 0 & -m_{23} & m_{22} \\ 0 & -m_{33} & m_{32} \end{bmatrix} \\ i \cdot \text{mod}(4) = 3 & \begin{bmatrix} 0 & m_{12} & m_{13} \\ 0 & m_{22} & m_{23} \\ 0 & m_{32} & m_{33} \end{bmatrix} \end{cases} \quad (7)$$

C. Drift compensation

Determining the orientation and cancelling the drift will be done by exploiting the cyclical behavior of running. The main idea revolves around the following assumption: If a person is running with a constant speed along a straight line, the cycles and its values should be similar to respectively the other cycles and its values. Therefore in the orientation estimation the same phases in different cycles should estimate the same orientation.

The first method will remove the mean of the angular velocity. The second method rotates the angular velocity to the axis on the knee perpendicular to the sagittal plane. The third method will instead of removing the mean, set a custom offset such that the drift is minimized.

In each method, the signal was truncated to a full number of cycles. Note that a cycle is defined as one whole period of a gait cycle that starts and end with the same event, the

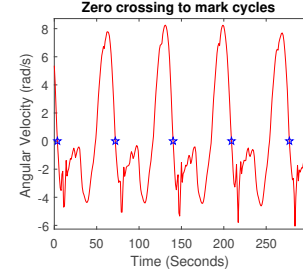


Fig. 3. Marking the cycles of $\omega_{s,y}$ using zero crossing on the falling edge of the signal.

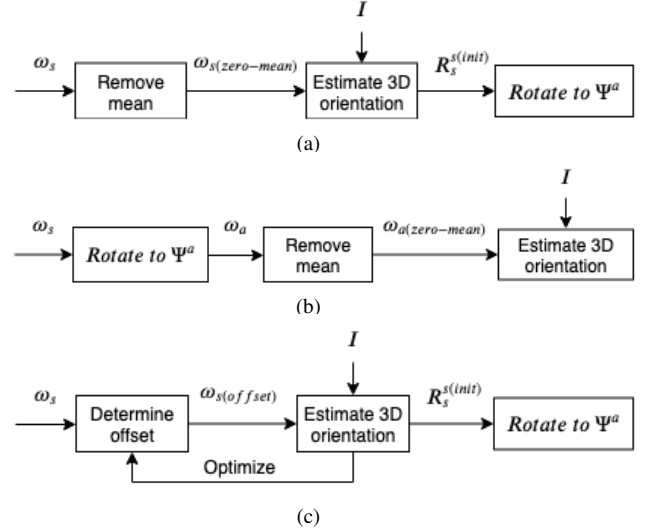


Fig. 4. The approach for each method. (a) shows method 1, (b) shows method 2 and (c) shows method 3.

method should work for any event that is distinguishable in the measured angular velocity data. The axis with the most dominant rotation around the axis on the knee perpendicular to the sagittal plane was used to truncate the signal. This was done by using the zero crossing of the falling edge, this is just before the leg comes in contact with the ground. In this work the axis was $\omega_{s,y}$. Due to the sampling frequency, a sample point with the value zero is not always defined, therefore the closest value is marked as the zero crossing. The marking is shown in Fig. 3.

1) *Method 1: Mean subtraction:* Since each cycle is expected to be very similar, there will be almost no variation between the cycles in the measured data. It is expected that this holds for the estimated orientation too. It is assumed that any bias in the measured data would result in a linear deviation in the orientation. Over a whole number of cycles, the mean of the measured data should therefore be equal to zero. This situation is mathematically described in (5). By subtracting the mean, the linear drift may be removed.

This zero-mean angular velocity $\omega_{s(\text{zero-mean})}$ will be integrated using the differential equation (1) with the identity matrix I as initial orientation to acquire the orientation of the sensor with respect to the initial orientation. To compare this method with the following two methods, the orientation will be rotated with \mathbf{R}_s^a to a partial segment coordinate frame with the same rotation matrix as used in method 2.

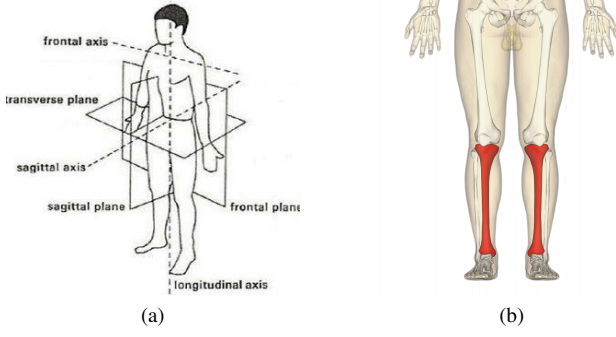


Fig. 9. (a) Anatomical planes of the human body. Source: [18]. (b) Location of the tibia (red) in the human body. Source: [19]

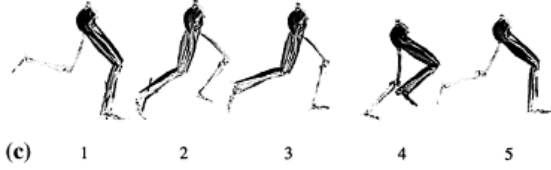


Fig. 10. Running phases: 1. Stance phase absorption. 2. Stance phase generation. 3. Swing phase generation. 4. Swing phase reversal. 5. Swing phase absorption. Source: [20]

APPENDIX

A. The human body

The human body can be divided into three orthogonal planes, in this paper they are referred to as the frontal plane, the transverse plane and the sagittal plane. See Fig. 9a. The direction of forward movement is perpendicular to the frontal plane, towards the front of the body.

As mentioned in the introduction, a minimal set of three sensors is chosen to identify and detect risks during running. In this research the method is only applied on the motions of the tibia, see Fig. 9b and 5. It is expected that during running the most variance in angular velocity of the tibia, is around the axis on the knee perpendicular to the sagittal plane. It is assumed that when a person stands straight, the tibia is aligned perpendicular to the transverse plane.

During running, several phases in the gait cycle can be differentiated, as pictured in Fig. 10. It is important to identify these phases in the measurement data to distinguish each running cycle. It is expected that between the swing phase absorption (5) and the stance phase absorption (1) a peak will be measured by the accelerometer due to the impact of the leg hitting the ground. It is expected that the gyroscope measures a peak during the swing phase, depicted as 3 in the figure.

B. Derivation drift analysis

This section shows the derivation of equations (5), (6) and (7). The differential equation for the 3D orientation estimation is:

$$\dot{\mathbf{R}}_s^{s,init} = \mathbf{R}_s^{s,init} \cdot \tilde{\boldsymbol{\omega}}_s^{s,init} \quad (9)$$

$$(10)$$

Where $\tilde{\boldsymbol{\omega}}_s^{s,init}$ is the skew-symmetric matrix:

$$\tilde{\boldsymbol{\omega}}_s^{s,init} = \begin{bmatrix} 0 & -\omega_z & \omega_y \\ \omega_z & 0 & -\omega_x \\ -\omega_y & \omega_x & 0 \end{bmatrix} \quad (11)$$

The meaning of (11) and (9) are explained in Section II-A. For the following derivations the notation of the reference frame is omitted. Equation (5) is the result of the first iteration of the following matrix multiplication with an initial rotation matrix. The measured angular velocity consists out of the ideal angular velocity and the error in the offset, $\omega_{e,x} = \omega_x + b_e$. Note that since the derivation is only one iteration of the differential equation, the unique angular velocities for every iteration are omitted for this derivation.

$$\dot{\mathbf{R}}_1 = \begin{bmatrix} m_{11} & m_{12} & m_{13} \\ m_{21} & m_{22} & m_{23} \\ m_{31} & m_{32} & m_{33} \end{bmatrix} \cdot \begin{bmatrix} 0 & -\omega_{e,z} & \omega_{e,y} \\ \omega_{e,z} & 0 & -\omega_{e,x} \\ -\omega_{e,y} & \omega_{e,x} & 0 \end{bmatrix} \quad (12)$$

$$\dot{\mathbf{R}}_1 = \begin{bmatrix} m_{12}\omega_{e,z} - m_{13}\omega_{e,y} & m_{13}\omega_{e,z} - m_{11}\omega_{e,x} \\ m_{22}\omega_{e,z} - m_{23}\omega_{e,y} & m_{23}\omega_{e,z} - m_{21}\omega_{e,x} \\ m_{32}\omega_{e,z} - m_{33}\omega_{e,y} & m_{33}\omega_{e,z} - m_{31}\omega_{e,x} \\ m_{11}\omega_{e,y} - m_{12}\omega_{e,x} \\ m_{21}\omega_{e,y} - m_{22}\omega_{e,x} \\ m_{31}\omega_{e,y} - m_{32}\omega_{e,x} \end{bmatrix} \quad (13)$$

In equation (6) and (7) only a 1D rotation about one axis exists. For this derivation the axis is the x-axis, but the derivation is similar for the other two axes. This results in the following matrix multiplications:

$$\dot{\mathbf{R}}_1 = \begin{bmatrix} m_{11} & m_{12} & m_{13} \\ m_{21} & m_{22} & m_{23} \\ m_{31} & m_{32} & m_{33} \end{bmatrix} \cdot \begin{bmatrix} 0 & 0 & 0 \\ 0 & 0 & -\omega_{e,x,1} \\ 0 & \omega_{e,x,1} & 0 \end{bmatrix} \quad (14)$$

$$\dot{\mathbf{R}}_2 = \begin{bmatrix} 0 & m_{13}\omega_{e,x_1} & -m_{12}\omega_{e,x_1} \\ 0 & m_{23}\omega_{e,x_1} & -m_{22}\omega_{e,x_1} \\ 0 & m_{33}\omega_{e,x_1} & -m_{32}\omega_{e,x_1} \end{bmatrix} \cdot \begin{bmatrix} 0 & 0 & 0 \\ 0 & 0 & -\omega_{e,x,2} \\ 0 & \omega_{e,x,2} & 0 \end{bmatrix} \quad (15)$$

$$\dot{\mathbf{R}}_3 = \begin{bmatrix} 0 & -m_{12}\omega_{e,x_1}\omega_{e,x_2} & -m_{13}\omega_{e,x_1}\omega_{e,x_2} \\ 0 & -m_{22}\omega_{e,x_1}\omega_{e,x_2} & -m_{23}\omega_{e,x_1}\omega_{e,x_2} \\ 0 & -m_{32}\omega_{e,x_1}\omega_{e,x_2} & -m_{33}\omega_{e,x_1}\omega_{e,x_2} \\ 0 & 0 & 0 \\ 0 & 0 & -\omega_{e,x,3} \\ 0 & \omega_{e,x,3} & 0 \end{bmatrix} \quad (16)$$

A pattern exists, as the first column of $\dot{\mathbf{R}}_i$ is always 0 and the constant of the initial rotation matrix is alternating between the second and third column. The signs of the columns are switched every two iterations. With this knowledge the product of the unique angular velocities and the signs and constants of the initial rotation matrix can be generalized.